Solid State Sciences 135 (2023) 107088

Contents lists available at ScienceDirect

Solid State Sciences

journal homepage: www.elsevier.com/locate/ssscie

Synthesis, properties and applications of novel inorganic yellow pigments based on Ni-doped Al_2TiO_5

Yi Wang [a], Peng Jiang [a,*], M.A. Subramanian [b], Wenbin Cao [a]

[a] Department of Inorganic Nonmetallic Materials, School of Materials Science and Engineering, University of Science and Technology Beijing, Beijing, 100083, China
[b] Department of Chemistry, Oregon State University, Corvallis, OR, 97330, USA

ARTICLE INFO

Keywords:
Pseudobrookite
Yellow pigment
Optical properties
Green alumina ceramic

ABSTRACT

Single phase $Al_{2-2x}Ni_xTi_{1+x}O_5$ ($0 \leq x \leq 0.4$) solid solutions were successfully synthesized by solid-phase reaction. The color of the compounds varied from yellow ($x = 0.1$) to turmeric ($x = 0.4$) with increasing nickel content. X-ray photoelectron spectroscopy analysis confirmed that the oxidation state of Ni is +2. The UV–Vis absorption spectrum showed that the color of the sample comes from the *d-d* transition of Ni^{2+} in octahedral coordination. Owing to excellent high temperature stability, the as-prepared oxide powders (10 wt%) were mechanically mixing with Al_2O_3 by conventional ball milling to prepare colored alumina ceramics. When Al_2O_3 is in excess, the blue $NiAl_2O_4$ impurity phase appeared, contributing to an intense green color of the Al_2O_3 ceramics composite. The Vickers micro hardness value of green alumina was higher than that of pure white alumina. The as-prepared samples were also dispersed in PMMA and bright yellow polymer composites were obtained, indicating great potential in polymer colorant.

1. Introduction

Inorganic pigments are commonly used in various fields such as plastics, paintings, ceramics, coatings and inks due to their thermal and chemical stability, weather resistance and high hiding power [1–3]. Among them, yellow pigments are important due to high visibility and primary color. However, most inorganic yellow pigments in use today, such as CdS and $PbCrO_4$, contain highly toxic elements which result more and more restricted application condition [4,5]. Thus the search for environmentally benign substitutes becomes a research focus in inorganic yellow pigments.

Some of Bi based oxides exhibit yellow colors. $Bi_4Zr_3O_{12}$, Bi_2O_3–ZnO–CaO, are widely used in the functional ceramic industry because of their non-toxic and environmentally friendly properties [6,7]. But the reserves of Bi is very limited in the earth's crust. In addition, the boiling points of bismuth oxides are low, indicating poor high temperature stability. Another solution is rare earth element-based yellow pigments. A series of new yellow pigments $Sr_{1-x}Ce_xMoO_4$ ($x = 0$–0.5) were synthesized by low temperature hydrothermal method. With the increase of Ce^{3+} substitution, the color of the synthesized product changed from white to yellow, with the b^* value, which represents the yellow hue, increased from −2.46 to 30.34 [8]. Chen studied thermal insulation pigments prepared from Ce-doped $Y_3Al_5O_{12}$, which shows bright yellow color. The product is light yellow to dark yellow with a maximum b^* value of 47.56 [9]. A new type of environment-friendly solid-phase yellow mixed oxide inorganic pigment is composed of Bi_2O_3–ZnO–CeO_2. Its color changes from orange to yellow as the temperature increases [10]. $BaSn_{1-x}Tb_xO_3$ were synthesized by adding Tb_4O_7 to the calcined mixture of SnO_2 and $BaCO_3$ or $BaSO_4$. When Tb concentration was 0.2 and 0.3, brighter yellow pigments were obtained [11]. Raj also prepared Tb-doped Sr_2MO_4 (M = Zr, Sn) yellow pigments with a good satisfied hue ($b^* = 53.4$) [12]. A series of environmentally friendly new inorganic pigments based on Bi^{3+} doping and Bi^{3+}/Tb^{3+} co-doping $LaYO_3$ were synthesized by a sol-gel method. The color of the synthesized product changes from light yellow to brown, and its b^* value is increased from 1.21 to 34.88 [13]. Although the prepared yellow pigments doped with rare earth elements have excellent coloring properties and environmental friendly, the limited storage and difficult separation of rare earth elements are bottleneck problems for many industrial productions.

Hence, transition metal ions as the chromophores are attempted in recent studies on low-cost yellow pigments. Different yellow colors are observed in oxides with Ni^{2+} in octahedral coordination. Shannon rationalized the root of yellow color in nickel oxide: when Ni^{2+} enters the highly distorted octahedral positions, the bright yellow color is

* Corresponding author.
E-mail address: jiangp@ustb.edu.cn (P. Jiang).

https://doi.org/10.1016/j.solidstatesciences.2022.107088
Received 30 October 2022; Received in revised form 1 December 2022; Accepted 12 December 2022
Available online 14 December 2022

produced [14]. A bright yellow and high UV–Vis–NIR reflectance nickel titanate ($NiTiO_3$) nanoparticle was obtained by pyrolysis of a polymer precursor [15]. A novel Ni-doped $BaTi_5O_{11}$ bright yellow pigment was successfully synthesized by solid-phase method [16]. Llusar et al. prepared and studied Ni-doped MgO–TiO_2 system ceramic pigments. In Ni–$MgTiO_3$ ilmenite, in which [MgO_6] and [TiO_6] octahedra are ordered alternately, the sintered pigment exhibits an intense yellow color. The generation of its color is related to the Ni^{2+} ions in the twisted octahedron [17]. Mg_2TiO_4 belongs to an inverse spinel structure with Mg^{2+} being equally distributed in octahedral and tetrahedral sites. In this spinel, Ni^{2+} ions preferentially substitute Mg^{2+} octahedral sites to give a yellow color [18]. In the $MgTi_2O_5$ pseudobrookite structure, Ni^{2+} ions replace [MgO_6] octahedral Mg sites [19]. With the increase of Ni content, the color changes from light yellow to orange-yellow. The structure of titanium pseudobrookite can accommodate many different metals in its two distinct and twisted octahedral cation sites. The special structural diversity of titanium pseudobrookite and its high refractoriness make it an excellent candidate for the development of new pigments.

Aluminum titanate Al_2TiO_5, crystallizes in the same structure as $MgTi_2O_5$. According to its color development mechanism, it provides a possibility for the preparation of yellow inorganic pigments by Ni-doped Al_2TiO_5. Low expansion, high melting point aluminum titanate material has become one of the best quality ceramic materials. It can be used as a high temperature pigment binder for corrosion resistance and high temperature resistance of glass melts. At the same time, the ion doping can effectively inhibit the decomposition of aluminum titanate [20–22]. Therefore, aluminum titanate is expected to become an ideal high-temperature ceramic substrate.

Aluminum titanate belongs to the orthorhombic pseudobrookite structure, and the space group is *Cmcm* (63). In the aluminum titanate structure, as shown in Fig. 1, aluminum ions (Al^{3+}) and titanium ions (Ti^{4+}) are uniformly distributed in a ratio of 1:1. [AlO_6] and [TiO_6] octahedra constitute the structural unit crystals of aluminum. The two distinct octahedra are highly twisted, randomly distributed and cross-connected in a co-edge or co-top structure [23].

Due to the extraordinary structural flexibility provided by the orthogonally symmetric structure in Al_2TiO_5, several transition metal ions were introduced in searching for new ceramic color pigments. Co, Cr and Mn substitution into Al_2TiO_5 showing pink, green and brown colors were successfully prepared through aerosol pyrolysis method [24]. Ni^{2+} were also doped into Al_2TiO_5 by sol-gel method and solid-phase method before [25]. However, unlike the other oxides with Ni^{2+} in [TiO_6] which show yellow hues, the prepared Ni–Al_2TiO_5 was reported to exhibit emerald to green color. $NiAl_2O_4$ impurity which gave a strong blue color appeared and the synthesized pigment was actually a mixed phase. As stated above, Ni^{2+} in octahedral sites normally contributes to a yellow color. Therefore, it is necessary to try to synthesize a single phase Ni–Al_2TiO_5 and clarify its true color.

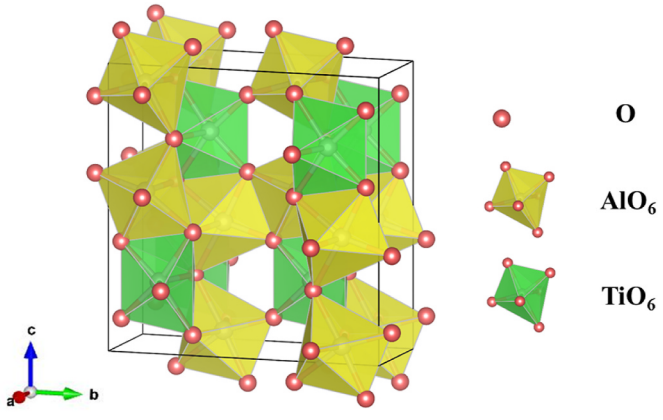

Fig. 1. Crystal structure of Al_2TiO_5.

To avoid the impurity of $NiAl_2O_4$, the valence state of ions was taken into consideration as a priority to design the formula. This is supposed to be compensated by the formation of oxygen vacancies in the structure. However, the appearance of $NiAl_2O_4$ indicates that the formation of $NiAl_2O_4$ is easier than creating oxygen vacancies in the structure. Therefore, in this work, each nickel ion replaces two aluminum ions and adds one titanium ion, contributing to a composition of $Al_{2-2x}Ni_xTi_{1+x}O_5$. In this way Ni–Al_2TiO_5 yellow powders with single phase XRD patterns were obtained.

The properties of the synthesized pigments were characterized by X-ray diffraction (XRD), X-ray photoelectron spectroscopy (XPS) and UV–Vis–NIR absorption spectroscopy. The synthesized compounds were dispersed in poly (methyl methacrylate) (PMMA) and alumina ceramics and their color properties were evaluated for pigment applications.

2. Experimental

2.1. Pigments preparation

$Al_{2-2x}Ni_xTi_{1+x}O_5$ $(0 \le x \le 0.4)$, compounds were prepared from stoichiometric amounts of Al_2O_3 (99.99% purity, Aladdin, China), TiO_2 (99.99% purity, Macklin, China), NiO (99.95% purity, Aladdin, China) by conventional solid-state synthesis. The raw materials were mixed and thoroughly ground using an agate mortar. Next, the mixed powders were pressed into pellets under an applied pressure of 10 MPa for 3 min. After that, the pellets were spread in alumina crucibles and calcined at 1500 °C for 2 h in air.

2.2. PMMA composite preparation

BPO (benzoyl peroxide, 10.0 mg, AR purity, Aladdin, China) was dissolved in MMA (methyl methacrylate, 10.0 mL, 99.0% purity, Aladdin, China) in a glass flask. After BPO was fully dissolved, the as-synthesized pigments (200 mg) were dispersed into the mixture of BPO and MMA. The flask was then placed in a water bath at 85 °C under magnetic stirring until the viscosity of MMA was close to glycerin. Then the thicker liquid was transferred into a glass tube, and the tube was placed into an oven. After 24 h of solidification at 50 °C and 1 h of final reaction at 100 °C, as a result, the rigid Poly (methyl methacrylate) (PMMA) stick was obtained. Both sides of the pigmented PMMA sticks were polished using fine (200–2000 grade) emery paper.

2.3. Green ceramic composite preparation

10 wt% of each pigment was thoroughly ground via a bench-top planetary automatic ball mill (MSK-SFM-1) with 300 rpm for 10 h with Al_2O_3 (99.99% purity). Then two-thirds of the volume of the tank filled with ethanol was added for ball milling and the powders were wet ground for another 30 min. After that, the samples were dried in a constant-temperature oven at 60 °C for 12 h. Subsequently, the powder mixtures were pressed into pellets under an applied pressure of 10 MPa and then sintered at 1500 °C for 6 h in air.

2.4. Characterization

Powder X-ray diffraction was completed on a Rigaku Ultima IV X-ray diffractometer under a Cu Kα ($\lambda = 1.5406$ Å) radiation in a 2θ range from 10° to 90° with a scanning speed of 20°/min and a step size of 0.02° operating at 40 kV and 40 mA.

The oxidation state of the Ni in the $Al_{2-2x}Ni_xTi_{1+x}O_5$ was analyzed by X-ray photoelectron spectroscopy (XPS, ESCALAB 250XI).

The morphology analysis and chemical composition of the pigment powders and alumina ceramics were studied using field emission scanning electron microscopy (FESEM, GeminiSEM 500) and energy dispersive spectrometer (EDS, Oxford X-Max). The surface of alumina ceramics was polished with diamond paste to 0.5 μm and thermal

etching before observation.

Colors can be defined precisely using the CIE L^* a^* b^* color space, which is a three-dimensional model. In CIE L^* a^* b^* system, L^* shows the brightness (black (0) to white (100)), a^* represents a green ($a^* < 0$)/red ($a^* > 0$) component and b^* stands for a blue ($b^* < 0$)/yellow ($b^* > 0$) component. L^* a^* b^* color coordinates were measured by a benchtop spectrometer (X-Rite Ci7600).

The UV–Vis–NIR absorbance spectra were acquired in the wavelength range of 200–2000 nm at room temperature with a UV–Vis–NIR spectrometer (Hitachi UH4150), where barium sulfate ($BaSO_4$) was employed as the reflectance standard.

The Vickers micro hardness (HV) of the alumina ceramics were measured on the polished surface, with a load of 300 gf and a dwell time of 15 s, using a Vickers hardness tester (EM-1500 L). Each sample took 10 points for record.

3. Results and discussion

3.1. The analysis of Ni-doped Al_2TiO_5 oxides

3.1.1. XRD analysis

The XRD patterns of the synthesized $Al_{2-2x}Ni_xTi_{1+x}O_5$ samples are shown in Fig. 2. The diffraction peaks of all synthesized samples can be indexed to the orthorhombic phase with space group *Cmcm* (63) (PDF#81–0030). The diffraction peaks in the figure are all sharp, indicating good crystallinity. Compared with the standard peak of $NiAl_2O_4$, the XRD pattern of nickel-containing compounds have no obvious peak at the main peak position of $NiAl_2O_4$ ($2\theta = 31.7°$, $37.2°$, $44.5°$), indicating that the synthesized samples do not contain nickel aluminate phase. At the same time, with the increase of Ni ion doping, the peaks in the XRD patterns shift to the left side as Ni^{2+} replaces Al^{3+} in the octahedral sites. As the sintering condition is in air and Ni^{2+} is the most stable state, Ni is assumed to exist in Ni^{2+} state. This is also based on the starting point of charge balance in original design. The ionic radius of Ni^{2+} is larger than that of Al^{3+}($R^{2+}_{Ni} = 0.69$ Å > $R^{3+}_{Al} = 0.54$ Å) [26,27], resulting in a larger lattice constant and a steady peak shift to the low angle region. This peak shift confirms the diffusion of Ni ions into Al_2TiO_5 to form a solid solution.

The introduction of Ni^{2+} ion tunes the color of the compound to be yellow. Fig. 3 shows the objective color of pigments. With the increase of nickel content, the color of the compound changes from light yellow to brownish yellow.

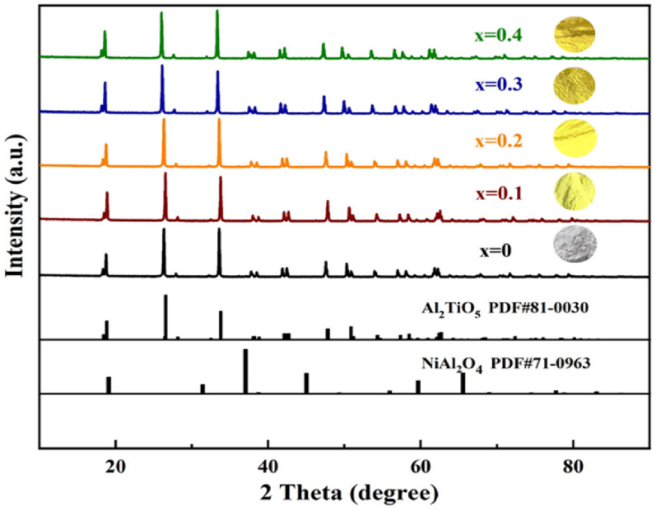

Fig. 2. XRD patterns of synthesized $Al_{2-2x}Ni_xTi_{1+x}O_5$ ($0 \le x \le 0.4$).

3.1.2. XPS analysis

X-ray photoelectron spectroscopy analysis was performed to further confirm the existence of Ni^{2+} in the compound. The XPS surveys of the $Al_{1.6}Ni_{0.2}Ti_{1.2}O_5$ and $Al_{1.2}Ni_{0.4}Ti_{1.4}O_5$ samples are shown in Fig. 4. Al, Ti, O, Ni are all derived from the target sample, and C is added during the test to calibrate the binding energy. The intensity of the peak increases with the increase of the doping amount. After fitting, the binding energy of the sample with $Al_{1.6}Ni_{0.2}Ti_{1.2}O_5$ consists of the main 2p 3/2 peak at 855.7 eV and the associated satellite peak at 861.7 eV. Similarly, the binding energy of $Al_{1.2}Ni_{0.4}Ti_{1.4}O_5$ consists of the 2p 3/2 peak at 855.4 eV and the associated satellite peak at 861.4 eV. Close binding energy values of Ni are obtained for the two samples with various Ni contents. A similar circumstance is Ni^{2+} in $Ni(OH)_2$, in which the main peak of Ni is located at 856.2 eV and the satellite peak is located at 861.2 eV [28]. Corresponding satellite peaks were also observed in NiO [29]. The binding energy of positively divalent Ni 2p 3/2 in octahedral coordination is reported to be 854.6 eV in Ni-doped $BaTi_5O_{11}$ [16]. Besides, the valence state of nickel ions in the octahedral structure of $BaMg_6Ti_6O_{19}$ is reported to be 855.61 eV [30]. In the paper, we can see that the binding energy of Ni^{3+} is 857.3 eV, which is higher than that of Ni^{2+}[31,32]. Above results confirm that nickel ions in $Al_{2-2x}Ni_xTi_{1+x}O_5$ ($0 \le x \le 0.4$) exist in the oxidation state of +2.

3.1.3. Optical properties analysis

The UV–Vis–NIR absorption spectra of all the synthesized samples are collected (shown in Fig. 5) to further prove the oxidation state and ligand environmental information of Ni, as metal ions situated in various oxidation states and ligands demonstrate distinct allowed absorption peaks based on the quantum theory. Al_2TiO_5 has only strong absorption below 400 nm. This indicates no absorption in the visible region, which results in white appearance. For Ni-doped Al_2TiO_5, the absorption band edge extends into the visible region (about 500 nm), and a larger red shift is observed with increasing Ni content. Apparently, the presence of nickel ions leads to the visible absorption of nickel-doped Al_2TiO_5. The absorption profiles of $Al_{2-2x}Ni_xTi_{1+x}O_5$ are following the features of Ni^{2+} doped $BaTi_5O_{11}$ and $MgTi_2O_5$ in octahedral coordination [16,19]. Ni^{2+} owns a $3d^8$ configuration, which only presents three spin-allowed transitions from its ground state $^3A_2$ (F) in an octahedral environment. For Ni doping (Fig. 5), the bands in the UV region are mainly due to the charge transfer transitions of O^{2-} - Ti^{4+} and O^{2-} - Ni^{2+}, and the first spin-allowed *d-d* transition of $^3A_2$ (F)→ $^3T_1$ (P) at 425 nm. The other two spin-allowed transitions are $^3A_2$ (F)→ $^3T_1$ (F) at 717 nm and $^3A_2$ (F)→ $^3T_2$ (F) at 1282 nm. As the nickel content increases, the strength of the absorption band at the shoulder will gradually increase, resulting in a more intense yellow color.

The results are reflected in the apparent color and CIE L^* a^* b^* color coordinates of the samples (Table 1). The color of Ni-doped pigments changed from light yellow to brownish yellow with the increase of doping amount. With the increase of doping element content, the L^* value gradually decreased, and the b^* value showed an upward trend.

3.2. Green alumina ceramics

3.2.1. XRD analysis of green alumina ceramics

Owing to high chemical and thermal stability, alumina ceramics are widely used in various application fields. Colored alumina ceramics are also used for decoration or protection. Wu et al. prepared the best Fe_2O_3 and TiO_2 co-doped corundum ceramics at 1440°C–1560 °C [33,34]. Tripathi et al. studied the mechanical properties of the mullite-alumina ceramics sintered at 1400°C–1600 °C with 2-6 wt% of ZrO_2 [35]. Considering the color performance and the mechanical property of Al_2O_3, the sintering temperature of colored alumina synthesis was set to be 1500 °C. Therefore, after the synthesis of yellow pigment powders, 10 wt% $Al_{2-2x}Ni_xTi_{1+x}O_5$ ($0 \le x \le 0.4$) and 90 wt% Al_2O_3 were mixed together to prepare color alumina ceramics through solid-phase

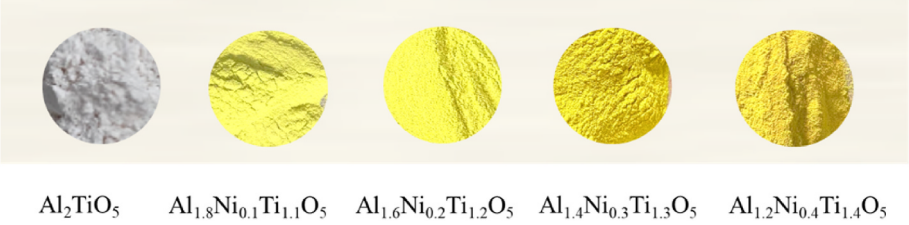

Fig. 3. The objective colors of pigments. (For interpretation of the references to color in this figure legend, the reader is referred to the Web version of this article.)

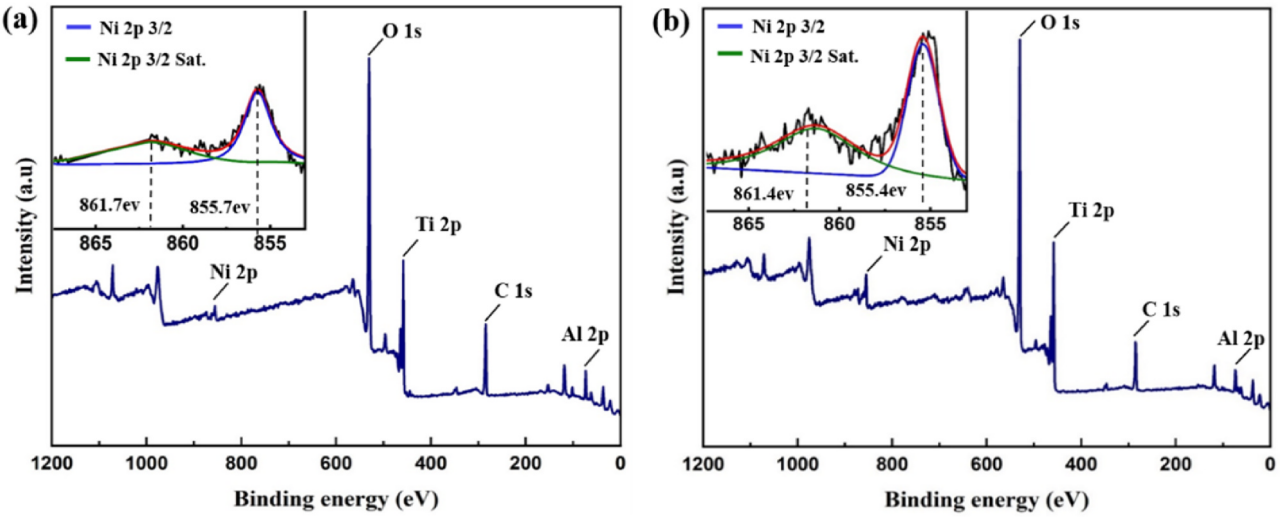

Fig. 4. XPS spectra of composite powders of (a) $Al_{1.6}Ni_{0.2}Ti_{1.2}O_5$ and amplified valence map of Ni ions and (b) $Al_{1.2}Ni_{0.4}Ti_{1.4}O_5$ and amplified valence map of Ni ions.

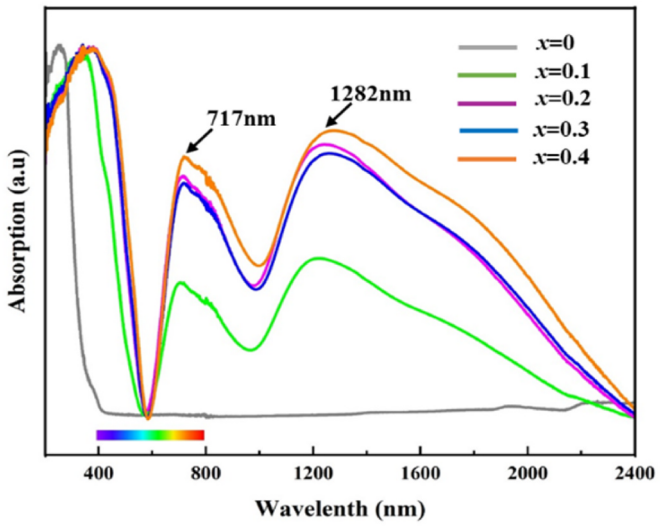

Fig. 5. UV–Vis–NIR absorbance spectra of $Al_{2-2x}Ni_xTi_{1+x}O_5$ ($0 \le x \le 0.4$).

Table 1
The CIE L^* a^* b^* color coordinates of the powder pigments.

$Al_{2-2x}Ni_xTi_{1+x}O_5$	L^*	a^*	b^*
$x = 0$	89.32	−1.03	4.16
$x = 0.1$	78.75	−7.83	39.33
$x = 0.2$	77.05	−4.09	45.24
$x = 0.3$	74.09	0.3	44.99
$x = 0.4$	71.2	3.62	42.54

reaction. The XRD patterns of the synthesized colored ceramics are shown in Fig. 6(a). Al_2O_3 phase and Al_2TiO_5 phase coexist in the as-synthesized alumina ceramic composite. The peak position of Al_2TiO_5 is lower due to less mass content. It can be seen that when the nickel content of the pigment increases, a small amount of TiO_2 is precipitated.

The $Al_{2-2x}Ni_xTi_{1+x}O_5$ ($0 \le x \le 0.4$) pigment powders demonstrate intense yellow color while the as-synthesized alumina ceramics show intense green hue. In order to clarify this color difference in the powder and the ceramic, an elevated amount of the pigment phase (10 wt%, 30 wt%, 50 wt%) were added into the ceramic composite and their XRD patterns are collected for analysis (Fig. 6(b)). With the increase of the pigment phase, $NiAl_2O_4$ impurity peaks appears and increase while the green color of the ceramic composite is slightly darker. Due to the strong blue tint of $NiAl_2O_4$, the ceramic pieces appear green with a mixture of blue and yellow. And this color is similar to the color of Ni–Al_2TiO_5 in previous report [25]. Although $NiAl_2O_4$ could be eliminated by charge compensation in the powder synthesis, when Al_2O_3 is in excess, it will reappear in Ni–Al_2TiO_5 and results in a green color. The impurity peak of $NiAl_2O_4$ can be clearly seen in the local profile ($2\theta = 31.7°$,$37.2°$, $44.5°$), and the impurity peak becomes stronger with the increase of pigment phase (Fig. 6(c)).

3.2.2. Microstructure of green alumina ceramics

The SEM and EDS of green alumina ceramics 10 wt% $Al_{1.6}Ni_{0.2}Ti_{1.2}O_5$ + 90 wt% Al_2O_3 are shown in Fig. 7. Clear grain and boundary are observed in the SEM image, but it was difficult to detect nickel by EDS analysis due to the small content of Ni in the prepared ceramics. For $Al_{1.6}Ni_{0.2}Ti_{1.2}O_5$ alumina ceramics, according to the EDS results summarized in Table 2, the bright grains are mainly composed of Al and O as well as Ti and a small amount of Ni. Because the matrix is alumina, the content of Al and O is high, and the other ratio is close to the theoretical value of $Al_{1.6}Ni_{0.2}Ti_{1.2}O_5$. In addition, the shape of bright

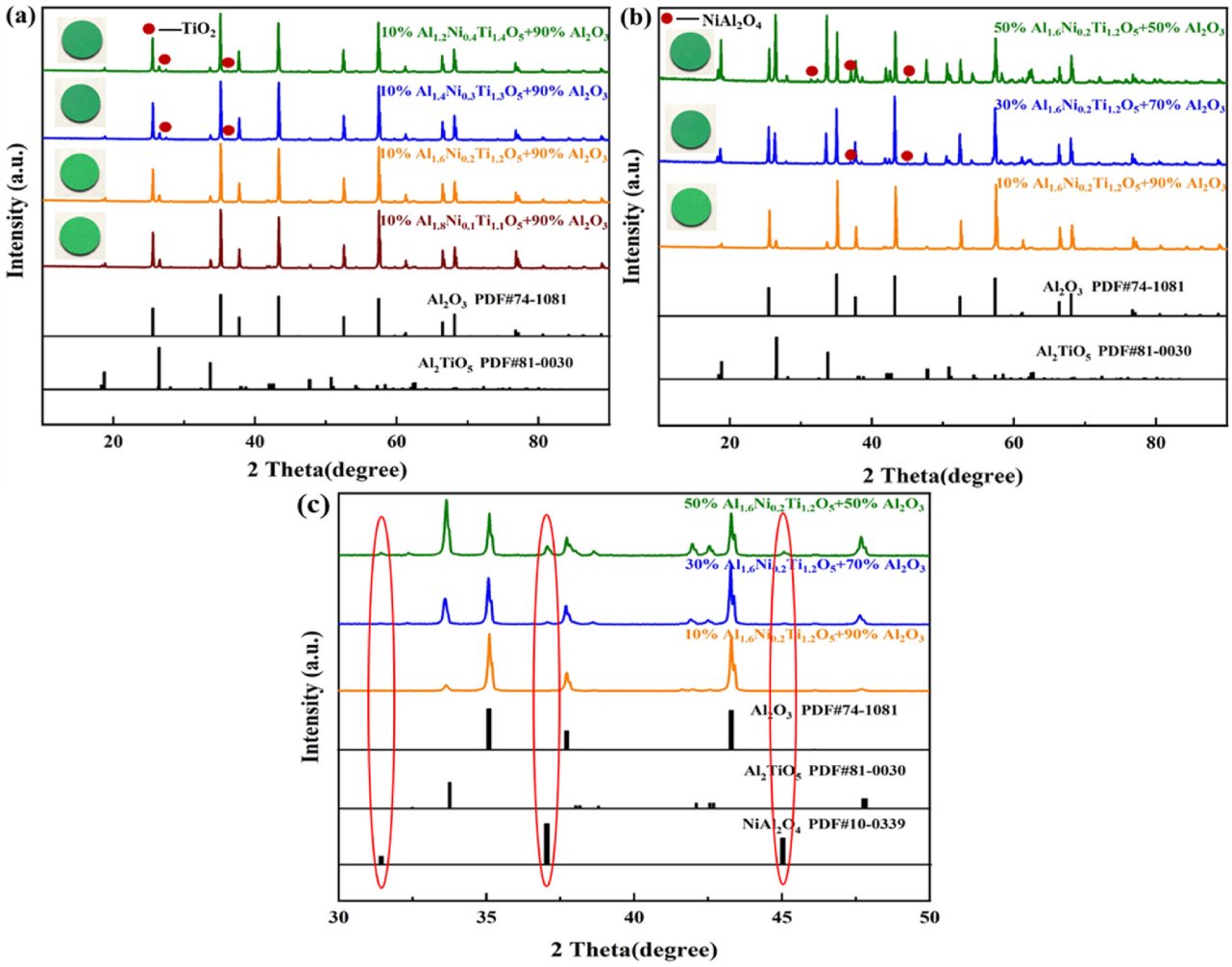

Fig. 6. The XRD patterns of (a) 10 wt% $Al_{2-2x}Ni_xTi_{1+x}O_5$ ($0 \leq x \leq 0.4$) + 90 wt% Al_2O_3; (b) 10 wt%, 30 wt%, 50 wt% $Al_{1.6}Ni_{0.2}Ti_{1.2}O_5$ + Al_2O_3; (c) XRD profiles of 10 wt%, 30 wt%, 50 wt% $Al_{1.6}Ni_{0.2}Ti_{1.2}O_5$ + Al_2O_3.

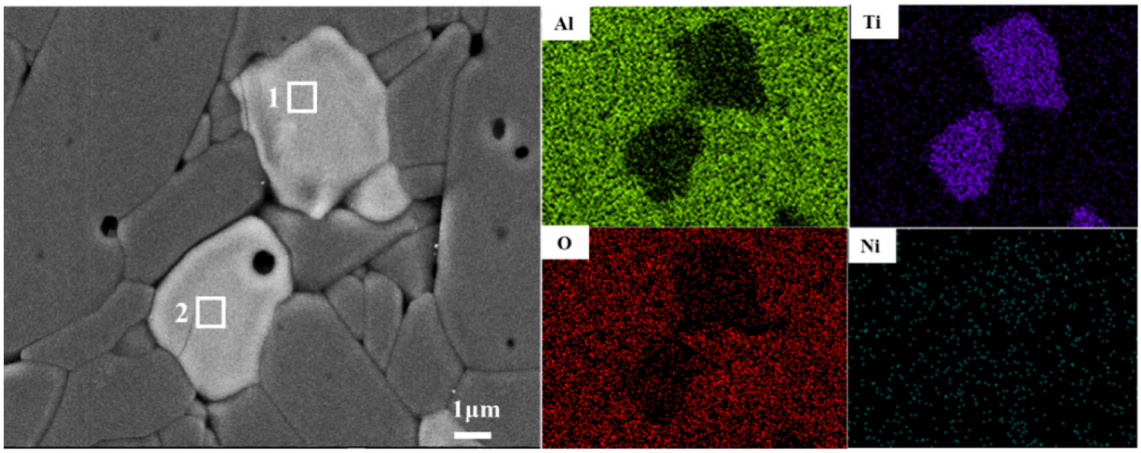

Fig. 7. SEM micrograph and EDS mapping of green alumina ceramics with 10 wt% $Al_{1.6}Ni_{0.2}Ti_{1.2}O_5$ and 90 wt% Al_2O_3. (For interpretation of the references to color in this figure legend, the reader is referred to the Web version of this article.)

grains in SEM images overlaps with EDS analysis. Thus, the bright grain was determined to be $Al_{1.6}Ni_{0.2}Ti_{1.2}O_5$. Therefore, the prepared Ni doped $Al_{1.6}Ni_{0.2}Ti_{1.2}O_5$ phase is stable after sintering with Al_2O_3 at high temperature.

3.2.3. *Mechanical properties of alumina ceramics*

The Vickers micro hardness of the colored alumina ceramics are characterized and compared with the white undoped alumina treated under the same sintering conditions, and the average value of Vickers hardness are shown in Fig. 8. When 10 wt% pigment was added to

Table 2
Multi-elemental atomic percentage (Unit: %) of points 1–2.

Element	Al	Ti	O	Ni	Total
1	22.62	12.62	64.24	0.52	100
2	22.74	12.84	63.96	0.46	100

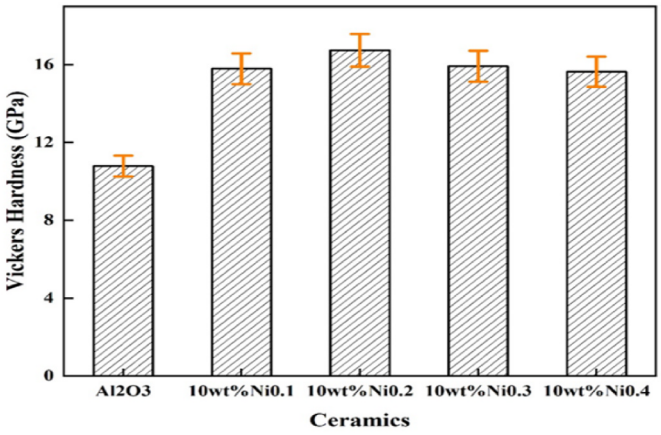

Fig. 8. The average Vickers hardness and the standard deviation to each point of green alumina ceramics with10 wt% $Al_{2-2x}Ni_xTi_{1+x}O_5$ ($0 \le x \le 0.4$) + 90 wt % Al_2O_3. (For interpretation of the references to color in this figure legend, the reader is referred to the Web version of this article.)

alumina ceramics, the hardness of nickel-doped colored alumina ceramics increased compared with pure alumina ceramics. The hardness of the composite ceramic made of the doping amount of 0.2 pigment and alumina reached the maximum value. With the increase of nickel doping content, the hardness of the samples showed a slight increase trend and then a slight decrease, indicating that the pigment has a favorable effect on the alumina hardness.

3.2.4. *Optical properties of green alumina ceramics*

Fig. 9 shows the objective color of alumina ceramics. Pure alumina ceramic is white, while the pigment-doped alumina is green. The green alumina ceramics prepared by compounding pigments and alumina have bright colors, and the coloring effect can be achieved by doping with a small amount of pigments. In the case of a certain doping content, with the increase of the nickel ion content in the pigment, the darker the green color is displayed by the alumina ceramic, with the smaller the value of a^* and L^* in the CIE value. These color properties are consistent with the sample results in the CIE L^* a^* b^* color coordinates. (Table 3). The pigment is yellow, the composite ceramic is green, and it's a^*, b^* values are reduced, as shown in Fig. 12, from the upper right corner to the lower left corner.

Fig. 10 shows the UV–Vis–NIR of $Al_{2-2x}Ni_xTi_{1+x}O_5$ ($0 \le x \le 0.4$) powders and their corresponding alumina ceramic composites. The pure alumina ceramics have nearly no absorbance in the 200–2400 nm region. When the pigments are introduced, colored alumina ceramics have associated absorption peaks at wavelengths in between 200 and 2400 nm. The absorption intensity increases slightly with the increase of the dopant ionic nickel content. The strongest light absorption occurs when the doping content is 0.4.

Table 3
The CIE L^* a^* b^* color coordinates of alumina ceramics.

sample	L^*	a^*	b^*
Al_2O_3	89.63	−4.32	5.23
10% $Al_{1.8}Ni_{0.1}Ti_{1.1}O_5$+90% Al_2O_3	73.79	−20.13	7.44
10% $Al_{1.6}Ni_{0.2}Ti_{1.2}O_5$+90% Al_2O_3	65.73	−26.01	9.4
10% $Al_{1.4}Ni_{0.3}Ti_{1.3}O_5$+90% Al_2O_3	64.61	−29.92	10.88
10% $Al_{1.2}Ni_{0.4}Ti_{1.4}O_5$+90% Al_2O_3	60.88	−30.83	11.49

Through phase analysis, we know that in the process of compounding with alumina, some Ni ions combine with alumina to form blue-green $NiAl_2O_4$ [36]. The absorption spectra of the samples in the 200–2400 nm wavelength range show strong absorption bands centered at 602 nm ($^3A_{2g} \rightarrow {}^1E_g$). Another strong absorption peak is located between 1008 nm and 1178 nm, which is due to the $^3A_{2g} \rightarrow {}^3T_{2g}$ transition of Ni2p ions in the octahedral crystal field (Fig. 10 (a)). Due to the production of impurity $NiAl_2O_4$, its absorption in the near infrared region is low, resulting in the final synthesis of green alumina ceramics in the near infrared region of the absorption strength is lower than that of the pigment phase. (Fig. 10 (b)). The absorption peak is more inclined to the result of the pigment phase and $NiAl_2O_4$. The final product absorbs in the yellow and red regions of the visible spectrum and therefore displays its complementary green color.

3.3. *Colored PMMA composite*

2 wt% Ni-doped Al_2TiO_5 compounds were dispersed in PMMA to prepare colored composites. The colors of the PMMA composites are shown in Fig. 11. The apparent color of the PMMA composites is uniform, which means that the low mass fraction of pigments has good stainability to PMMA. Fig. 12 provides a graphical representation of colored PMMA composites in the a^* b^* color space. With the increase of the doping amount, the a^* and b^* values of the samples increased continuously, which indicated that the yellow color gradually increased. The color coordinates of colored PMMA composites in CIE L^* a^* b^* are different from powder pigments, as better transparency is exhibited in colored PMMA composites. The color of the synthesized PMMA is consistent with the color of the pigment when viewed from the table. Therefore, a small amount of pigment doping can obtain yellow PMMA.

4. Summary and conclusions

In this work, the solid solution of Ni-doped Al_2TiO_5 was successfully prepared by solid-phase reaction. With the increase of doping ions, the solid solution finally showed a trend of changing from yellow-green to turmeric. Combining XPS and UV–Vis–NIR characterization, the origin of the color is attributed to the $^3A_2$ (F)→ $^3T_1$ (F) d-d spin-allowed transition of Ni^{2+} at 717 nm under octahedral coordination. Subsequently, colored alumina ceramics were prepared by mechanically mixing 10 wt% of each pigment with Al_2O_3 by conventional ball milling.

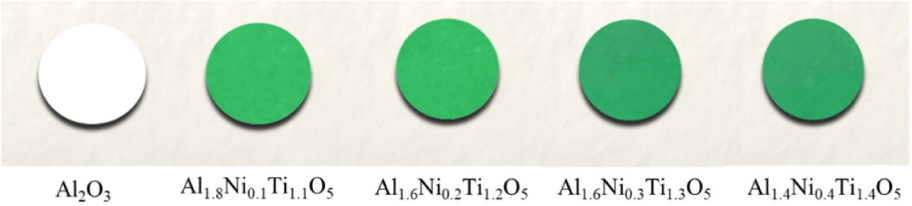

Fig. 9. The objective colors of alumina ceramics. (For interpretation of the references to color in this figure legend, the reader is referred to the Web version of this article.)

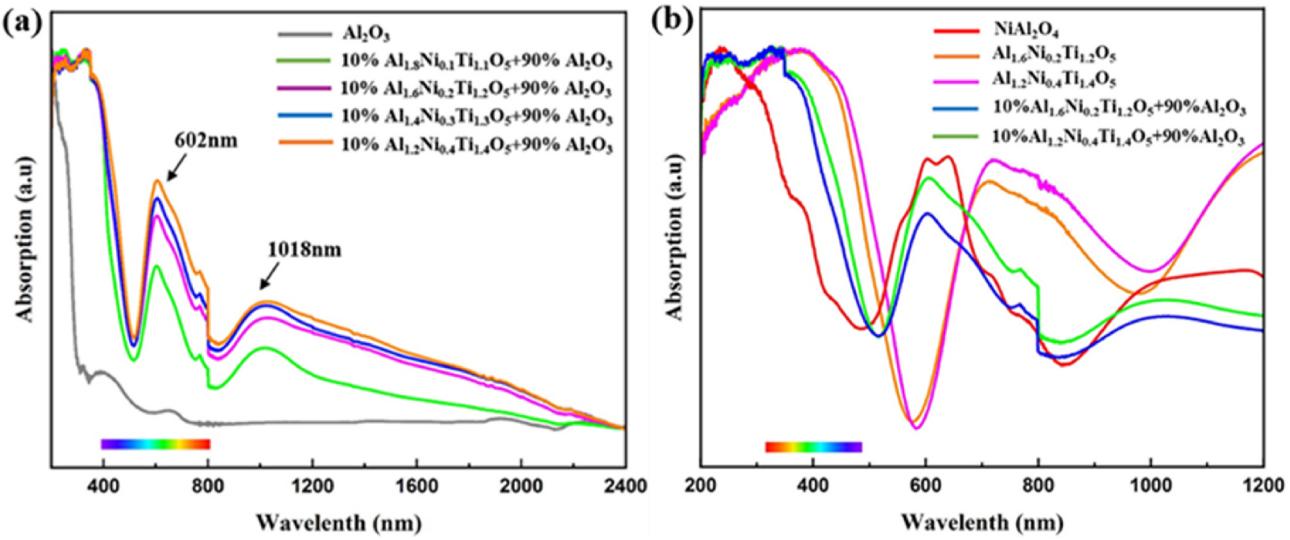

Fig. 10. UV–Vis–NIR absorbance spectra of (a) $Al_{2-2x}Ni_xTi_{1+x}O_5$ and alumina composite ceramics ($0 \leq x \leq 0.4$); (b) Ni-doped Al_2TiO_5 systems and $NiAl_2O_4$.

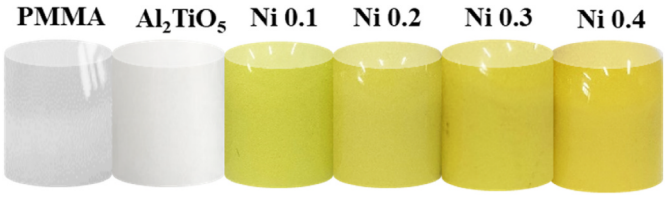

Fig. 11. Colors of pure PMMA and PMMA composite with 2 wt% Ni doped Al_2TiO_5 pigments. (For interpretation of the references to color in this figure legend, the reader is referred to the Web version of this article.)

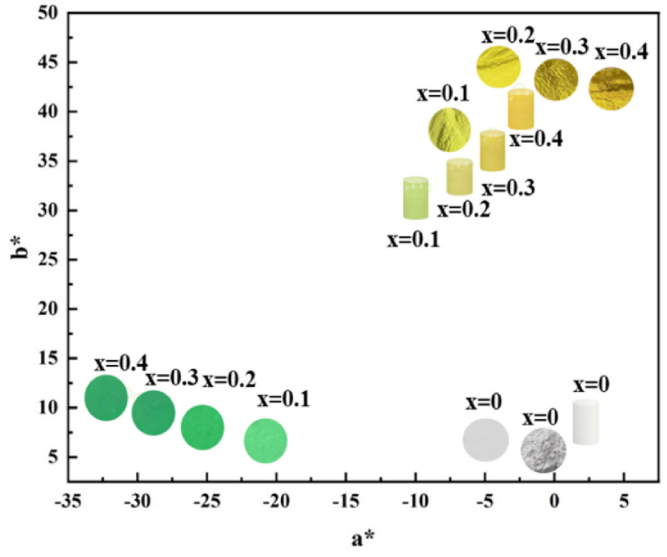

Fig. 12. Color coordinates and digital photographs of synthetic pigment powders, composite alumina ceramics, PMMA in a^* b^*space. (For interpretation of the references to color in this figure legend, the reader is referred to the Web version of this article.)

The Vickers micro hardness value of green alumina is higher than that of pure white alumina. With the addition of a small amount of pigment (10 wt%), the green alumina ceramics exhibited good optical properties. PMMA composites with 2 wt% pigments were also successfully prepared with desirable color properties, indicating their good adaptability to plastic coloring.

Author statement

P Jiang proposed the overall research direction and guided the project. P. Jiang and Yi Wang conceived the idea and designed the experiments, performed the materials synthesis, analyzed data, and drafted the manuscript. W. Cao and M. A. Subramanian gave valuable discussions and suggestions.

Declaration of competing interest

The authors declare that they have no known competing financial interests or personal relationships that could have appeared to influence the work reported in this paper.

Data availability

Data will be made available on request.

Acknowledgements

This work was supported by the National Natural Science Foundation of China under Grant No. 11230538, Youth Teacher International Exchange & Growth Program under the grant No. QNXM20220018. The work done at Oregon State University is supported by US National Science Foundation Grant No. DMR-2025615.

References

[1] B. Bae, Wendusu, S. Tamura, N. Imanaka, Novel environmentally friendly inorganic yellow pigments based on gehlenite-type structure, Ceram. Int. 42 (13) (2016) 15104–15106.
[2] S. Xiong, J.L. Kuang, Q. Zheng, Effects of Si/Al, Na/Al, and H_2O/Na_2O molar ratios on formaldehyde barrier properties of inorganic aluminosilicate coatings, Int. J. Miner. Metall. Mater. 28 (11) (2021) 1868–1874.
[3] H.Y. Zhao, J.L. Kuang, P. Sun, W.X. Liu, W.B. Cao, One-step hydrothermal synthesis of an orthorhombic $WO_3{\cdot}H_2O/TiO_2$ heterojunction and its photocatalytic activity, Mater. Sci. Forum 1072 (2022) 195–201.
[4] G. Del Nero, G. Cappelletti, S. Ardizzone, P. Fermo, Yellow Pr-zircon pigments: the role of praseodymium and of the mineralizer, J. Eur. Ceram. Soc. 24 (14) (2004) 3603–3611.
[5] P. Meenakshi, M. Selvaraj, Bismuth titanate as an infrared reflective pigment for cool roof coating, Sol. Energy Mater. Sol. Cell. 174 (2018) 530–537.

[6] T. Tsukimori, R. Oka, T. Masui, Synthesis and characterization of $Bi_4Zr_3O_{12}$ as an environment-friendly inorganic yellow pigment, Dyes Pigments 139 (2017) 808–811.
[7] S. Xu, J. Zhang, Y. Zhang, W. Zhu, A. Wang, S. Zhuang, High near-infrared reflectance Bi_2O_3-ZnO-CaO yellow pigment system, Ceram. Int. 48 (10) (2022) 14406–14413.
[8] V. Elakkiya, S. Sumathi, Low-temperature synthesis of environment-friendly cool yellow pigment: Ce substituted SrMoO4, Mater. Lett. 263 (2020) 127246–127254.
[9] Chen, A. Han, M. Ye, J. Wang, X. Chen, A new thermal insulation ceramic pigment: Ce-doped Y3Al5O12 compounds combined with high near-infrared reflectance and low thermal conductivity, J. Alloys Compd. 886 (2021) 161257, 160266.
[10] K. Těšitelová, P. Šulcová, Synthesis and study of mixed oxide inorganic pigment from Bi_2O_3-ZnO-CeO_2 system, J. Therm. Anal. Calorim. 130 (1) (2017) 57–62.
[11] P. Luňáková, M. Trojan, J. Luxová, J. Trojan, $BaSn_{1-x}Tb_xO_3$: a new yellow pigment based on a perovskite structure, Dyes Pigments 96 (1) (2013) 264–268.
[12] A. Raj, P. Prabhakar Rao, S. Divya, T.R. Ajuthara, Terbium doped Sr_2MO_4 [M=Sn and Zr] yellow pigments with high infrared reflectance for energy saving applications, Powder Technol. 311 (2017) 52–58.
[13] Y. Xiao, B. Huang, J. Chen, X. Sun, Novel Bi^{3+} doped and Bi^{3+}/Tb^{3+} co-doped $LaYO_3$ pigments with high near-infrared reflectances, J. Alloys Compd. 762 (2018) 873–880.
[14] G.R. Rossman, R.D. Shannon, K.W. Robert, Origin of the yellow color of complex nickel oxides, J. Solid State Chem. 39 (3) (1981) 277–287.
[15] J. Wang, Y. Li, Y. Byon, S. Mei, G. Zhang, Synthesis and characterization of $NiTiO_3$ yellow nano pigment with high solar radiation reflection efficiency, Powder Technol. 235 (2013) 303–306.
[16] J. Zou, P. Zhang, Ni-doped $BaTi_5O_{11}$: new brilliant yellow pigment with high NIR reflectance as solar reflective fillers, Ceram. Int. 46 (3) (2020) 3490–3497.
[17] M. Llusar, E. García, M.T. García, V. Esteve, C. Gargori, G. Monrós, Synthesis and coloring performance of Ni-geikielite (Ni, Mg)TiO_3 yellow pigments: effect of temperature, Ni-doping and synthesis method, J. Eur. Ceram. Soc. 35 (13) (2015) 3721–3734.
[18] M. Llusar, E. García, M.T. García, C. Gargori, J.A. Badenes, G. Monrós, Stability and coloring properties of Ni-qandilite green spinels (Ni, Mg)$_2TiO_4$: the "half color wheel" of Ni-doped magnesium titanates, Dyes Pigments 122 (2015) 368–381.
[19] M. Llusar, E. García, M.T. García, C. Gargori, J.A. Badenes, G. Monrós, Synthesis, stability and coloring properties of yellow-orange pigments based on Ni-doped karrooite (Ni, Mg)Ti_2O_5, J. Eur. Ceram. Soc. 35 (1) (2015) 357–376.
[20] C. Chen, H. Awaji, Temperature dependence of mechanical properties of aluminum titanate ceramics, J. Eur. Ceram. Soc. 27 (1) (2007) 13–18.
[21] M. Berger, A. Sayir, Directional solidification of Al_2O_3-Al_2TiO_5 system, J. Eur. Ceram. Soc. 28 (12) (2008) 2411–2419.
[22] J. Zhao, X. Hao, S. Wang, X. Zhang, Z. Wang, X. Luo, Z. Xie, J. Luo, Sintering behavior and thermal shock resistance of aluminum titanate (Al_2TiO_5)-toughened MgO-based ceramics, Ceram. Int. 47 (19) (2021) 26643–26650.
[23] G. Zhao, B. Yang, Q. Li, Aluminum titanate-calcium dialuminate composites with low thermal expansion and high strength, J. Alloys Compd. 656 (2016) 1–4.
[24] M. Dondi, T.S. Lyubenova, J.B. Carda, M. Ocaña, M-doped Al_2TiO_5(M=Cr, Mn, Co) solid solutions and their use as ceramic pigments, J. Am. Ceram. Soc. 92 (9) (2009) 1972–1980.
[25] J. Chen, G. Feng, F. Jiang, L. Yin, Q. Zhao, S. Lan, X. Zhang, J. Liu, Q. Hu, W. Jiang, Synthesis and coloring properties of novel Ni-doped tialite pigments, Ceram. Int. 47 (23) (2021) 33242–33251.
[26] R.K. Behera, A. Dutta, D. Ghosh, S. Bera, S. Bhattacharyya, N. Pradhan, Doping the smallest shannon radii transition metal ion Ni(II) for stabilizing alpha-CsPbI(3) perovskite nanocrystals, J. Phys. Chem. Lett. 10 (24) (2019) 7916–7921.
[27] N.M.A. Zulkafli, M.K. Yaakob, M.H. Ridzwan, M.F. Kasim, M.M. Mahat, R. Rajmi, M.H. Mamat, A.A. Mohamad, M.Z.A. Yahya, Insight into the role of atomic interaction and ionic radius in Al doped $BiFeO_3$: structural, electronic, and optical properties, Phys. B Condens. Matter 648 (2022).
[28] H. Nesbitt, D. Legrand, G. Bancroft, Interpretation of Ni2p XPS spectra of Ni conductors and Ni insulators, Phys. Chem. Miner. 27 (2000) 357–366.
[29] N. Jayababu, M. Poloju, J. Shruthi, M. Ramana Reddy, Semi shield driven p-n heterostructures and their role in enhancing the room temperature ethanol gas sensing performance of NiO/SnO_2 nanocomposites, Ceram. Int. 45 (12) (2019) 15134–15142.
[30] Q. Cheng, X. Chen, L. Liu, P. Jiang, D. Song, M.A. Subramanian, Synthesis and optical properties of Ni/Co/Cr doped $BaMg_6Ti_6O_{19}$, Ceram. Int. 47 (24) (2021) 34086–34091.
[31] Z. Fu, J. Hu, W. Hu, S. Yang, Y. Luo, Quantitative analysis of Ni^{2+}/Ni^{3+} in Li$[Ni_xMn_yCo_z]O_2$ cathode materials: non-linear least-squares fitting of XPS spectra, Appl. Surf. Sci. 441 (2018) 1048–1056.
[32] P.M. Lee, Y.J. Wu, C.Y. Hsieh, C.H. Liao, Y.S. Liu, C.Y. Liu, Observation of Ni^{3+} acceptor in P-type Ni(P):SnO_2, Appl. Surf. Sci. 337 (2015) 33–37.
[33] J. Wu, Y. Liu, X. Xu, S. Liu, The microstructures and properties of Fe_2O_3 and TiO_2 co-doped corundum ceramics for solar thermal absorbing materials, Ceram. Int. (2022).
[34] X. Xu, Q. Zhang, J. Wu, H. Wang, K. Tian, C. Wu, Preparation and characterization of corundum-based ceramics for thermal storage, Ceram. Int. 47 (16) (2021) 23620–23629.
[35] H.S. Tripathi, S.K. Das, B. Mukherjee, Synthesis and thermo-mechanical properties of mullite-alumina composite derived from sillimanite beach sand: effect of ZrO_2, Ceram. Int. 27 (8) (2001) 833–837.
[36] S.G. Menon, H.C. Swart, Microwave-assisted synthesis of blue-green $NiAl_2O_4$ nanoparticle pigments with high near-infrared reflectance for indoor cooling, J. Alloys Compd. 819 (2020) 152991–152998.